AIAA JOURNAL
Vol. 38, No. 11, November 2000

Boundary Correction Factors for Elliptical Surface Cracks Emanating from Countersunk Rivet Holes

Anisur Rahman*
Drexel University, Philadelphia, Pennsylvania 19104
and
John G. Bakuckas Jr.,† Catherine A. Bigelow,‡ and Paul W. Tan§
Federal Aviation Administration William J. Hughes Technical Center, Atlantic City International Airport, New Jersey 08405

To predict the crack growth and residual strength of riveted joints subjected to widespread fatigue damage, accurate stress and fracture analyses of corner and surface cracks at a rivet hole are needed. The results presented focus on the calculation of stress-intensity factor (SIF) solutions for cracks at countersunk rivet holes for tension, bending, and wedge load conditions. A wide range of configuration parameters were varied, including the crack size, crack shape, crack location, and length of the straight shank hole. A finite-element-based global–intermediate–local hierarchical approach was used. The results are expressed as boundary correction factors (BCFs), which are nondimensional representations of the SIF. The BCFs were determined along the crack front in terms of the physical angle, which was measured from the inner surface of the plate to a point on the hole boundary or on the outer surface of the plate. In general, the values of BCFs increased along the crack front, moving from the inner surface of the plate toward the hole boundary or the outer surface. The values of the BCFs were highest for the crack fronts closest to the hole boundary. The trends in the solutions were the same for the three loading conditions.

Introduction

ONGOING aging aircraft research activities are aimed at developing and implementing advanced fatigue and fracture mechanics concepts into the damage tolerance analysis methodology for the aging, current, and next generation fleets. These activities include developing methods to predict the onset of widespread fatigue damage (WFD). One of the objectives of the Federal Aviation Administration's National Aging Aircraft Research Program is to develop the methodology to predict crack initiation, crack growth rates, and residual strengths of aircraft structures susceptible to WFD. One of the fourteen possible locations susceptible to WFD identified by the Industry Committee on WFD is the riveted lap splice joint.[1] Multiple cracks can form in a riveted lap splice joint due to stress concentrations in the rivet holes. To reliably predict crack growth rates and fracture strengths of riveted joints susceptible to WFD, accurate stress-intensity factor (SIF) solutions of corner and surface cracks at a rivet hole are needed. Exact closed-form SIF solutions for cracks in three-dimensional solids are often lacking for complex configurations such as countersunk rivet holes; therefore, approximate solutions must be used. Over the past two decades, considerable effort has been placed on developing computationally efficient methods to provide accurate SIF solutions for cracks in three-dimensional bodies. These methods include conventional finite element method (FEM),[2–5] the finite element alternating method (FEAM),[6–8] the boundary element method (BEM),[9,10] and the three-dimensional weight function method (WFM).[11,12] With advances in pre and post processors and computer hardware and improvements in equation solvers, time savings are being realized in both geometry development and analysis of complex models. With the computational tools in place, much-needed SIF solutions required for damage tolerance assessments of cracked rivet holes can be obtained.

A recent experimental study[13] provides extensive experimental data on the crack front shape and fatigue growth of cracks from rivet holes in fuselage lap joint regions. Fatigue damage in an actual fuselage lap joint removed from a full-scale test article was characterized. An extensive database was established cataloging the damage state of the fuselage lap region including crack initiation, growth rates, size, location, and fracture morphology. Hidden cracks from rivet holes in the inner skin, outer skin, and tear straps were found during fractographic examinations. In the outer skin, cracking typically initiated from the rivet hole at the faying surface between the inner and outer skins due to fretting. Marker band analysis showed that the cracks typically grew beneath the surface with an elliptical shape, remaining hidden for a portion of their growth. The tunneling cracks penetrated the outer surface after growing to lengths of two-to-three-times the skin thickness.

To complement such experimental studies, SIF solutions would be useful in interpreting results as well as conducting damage tolerance assessments. However, few solutions exist for cracks at countersunk rivet holes. Some work has been done to generate SIF solutions for cracks in countersunk rivet holes.[5,8] However, many gaps exist in available SIF solutions and further work is required particularly for breakthrough crack configurations and solutions under bending and pin loading. This paper provides a summary of a recent work conducted to expand the available database of SIF solutions. A complete presentation of the results can be found in Rahman et al.[14] Configurations representing typical countersunk holes in aircraft structural joints were analyzed under tension, bending, and wedge loading conditions. The crack size, crack shape, and crack location were selected to represent real world scenarios. A global-intermediate-local (GIL) hierarchical approach based on the finite element method was used. Representative results for boundary correction factors calculated using the GIL approach are presented.

Configuration and Loadings

The configuration analyzed in this study was a countersunk rivet hole in a plate with a half-height to half-width ratio $H/W = 2$ as shown in Fig. 1a. The ratio of the straight-shank hole radius to plate half-width (W/R) was 5. For all calculations, the total angle subtended by the countersunk hole was 100 deg. The ratio of the length of the straight-shank portion of the hole to the plate thickness (h/t) was varied to values of 0.05, 0.25, and 0.50. Material with modulus of elasticity E and Poisson's ratio ν ($\nu = 0.3$) was used in this analysis. Three loading conditions were considered, a remote tension S_t, a remote bending S_b, and a line load P_y applied in the hole as shown in Figs. 1b, 1c, and 1d, respectively. The remote tension

Received 17 September 1999; revision received 12 January 2000; accepted for publication 27 March 2000.

*Research Assistant Professor, Department of Materials Engineering, 3141 Chestnut Street; rahmana@drexel.edu. Member AIAA.
†Research Engineer, Airframes Structures Section, AAR-431.
‡Manager, Airworthiness Assurance R&D Branch, AAR-430.
§Manager, Airframes Structures Section, AAR-431. Senior Member AIAA.

load was applied using a constant stress $S = S_t$ at $y = H$. The remote bending load was applied using a linear stress distribution at $y = H$. The value of stress applied at $y = H$ was given by

$$S = S_b(z/t) \tag{1}$$

This application of stress ensured an opening mode displacement of the crack surfaces. The line load (P_y), simulating a wedge load condition, was applied on the plane of symmetry of the countersunk hole. P_y and was defined as the vertical component of a traction load P_l acting normal to the surface, as shown in Fig. 1e. Thus the line load was given by

$$P_y = \begin{cases} P_l \cos 50 \text{ deg}, & 0 \le Z/t \le 1 - h/t \\ P_l, & 1 - h/t < Z/t \le 1 \end{cases} \tag{2}$$

Results presented in this study were normalized with respect to the modulus of elasticity by setting E to a unit value. The results were also normalized with respect to applied loading by setting S_t, S_b, and P_l, to unity. The five crack locations shown in Fig. 1f were analyzed. All cracks were elliptical with the center of the ellipse at the intersection of the straight-shank portion of the rivet hole and the inner surface of the plate. The size and shape of each crack were defined by a and c, the two elliptical axes, where a is parallel to the Z axis and c is parallel to the Y axis. At crack location 1, Fig. 1f, the crack is a corner crack, the value of a set to $h/2$, and h/t was set to 0.05, 0.25, and 0.5. At crack location 2, also a corner crack, a was set equal to h, and h/t was varied as before. At crack location 3, a breakthrough crack, a was defined such that the crack would intersect the surface of the rivet hole at $Z/t = (h + t)/2t$, and h/t was varied as before. At crack location 4, a through the thickness crack, a was defined such that the crack would intersect the surface of the rivet hole at $Z/t = 1$. For crack locations 1–4, a/c was set to 1, 0.75, and 0.5. At crack location 5, only one crack was analyzed, a breakthrough crack having $a/c = 1$ with $c/t = 3.125$. These cracking configurations were selected to represent typical scenarios observed during the fractographic examinations reported in Ref. 13. The full analysis matrix shown in Table 1 consists of 117 solutions.

Table 1 Analysis matrix

Parameter	Value
h/t	0.05, 0.25, 0.5
a/c	1.0, 0.75, 0.5
Locations	1, 2, 3, 4, and 5[a]
Loading conditions	Tension, bending, and wedge load

[a]For location 5, only $h/t = 0.05$ and $a/c = 1$ case is solved.

Definition of Stress-Intensity Factor

The mode I stress-intensity factor (K_I) at any location along the crack front under tensile loading is given as

$$K_I = S_t\sqrt{\frac{\pi a}{Q}}F_t\left(\frac{a}{t}, \frac{a}{c}, \frac{h}{t}, \frac{R}{t}, \theta\right) \tag{3}$$

for bending load

$$K_I = S_b\sqrt{\frac{\pi a}{Q}}F_b\left(\frac{a}{t}, \frac{a}{c}, \frac{h}{t}, \frac{R}{t}, \theta\right) \tag{4}$$

and for wedge load

$$K_I = S_w\sqrt{\frac{\pi a}{Q}}F_w\left(\frac{a}{t}, \frac{a}{c}, \frac{h}{t}, \frac{R}{t}, \theta\right) \tag{5}$$

where the wedge stress per unit area S_w is simulated using a normal line load P_l as

$$S_w = P_l/t \tag{6}$$

The boundary correction factors, F_t (tensile), F_b (bending), and F_w (wedge load), were calculated along the crack front for the various combinations of parameters (a/c, h/t, and crack location) shown in Table 1. The crack dimensions a and c and physical angle θ are defined in Fig. 1g. The physical angle θ is the angle between the back surface of the plate and a point on the crack front as indicated in Fig. 1g. The shape factor Q, is the square of the complete elliptic integral of the second kind. An approximation for the complete elliptical integral of the second kind is given by Rawe (see Ref. 15). The shape factor based on this approximation is

$$Q = 1 + 1.464(a/c)^{1.65} \quad \text{for} \quad a/c \le 1$$

$$Q = 1 + 1.464(c/a)^{1.65} \quad \text{for} \quad a/c > 1 \tag{7}$$

Global-Intermediate-Local Hierarchical Approach

The global-intermediate-local (GIL) hierarchical finite element approach, illustrated in Fig. 2, was used to obtain the boundary correction factors for the countersunk rivet holes. The GIL approach is an application of the finite element submodeling technique that was used to generate three-dimensional stress-intensity factors. The method was validated by Bakuckas[16] using a benchmark problem of a corner crack in a straight shank hole. The GIL approach was compared to several different computational methods: the fracture analysis code in three dimensions (FRANC3D), the WFM, the FEAM, the FEM with the equivalent domain integral (DIM), and the fracture analysis by distributed dislocation in three dimensions (FADD3D).

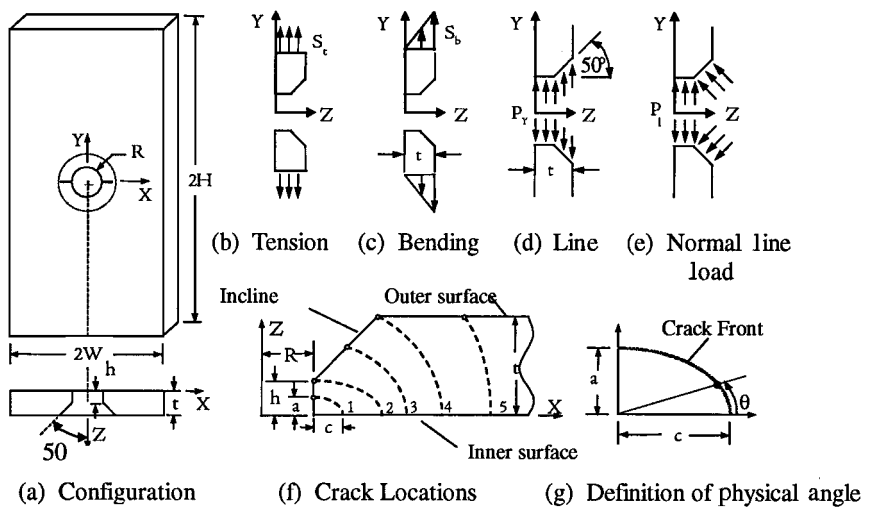

Fig. 1 Problem description.

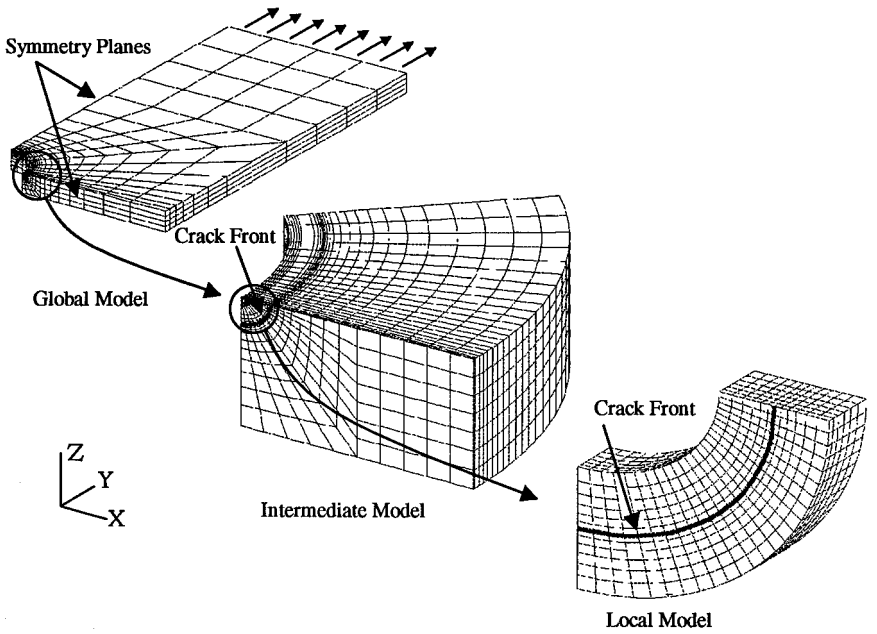

Fig. 2 GIL hierarchical approach.

The results were also compared with semi-empirical equations developed at NASA Langley Research Center. All of the results were in good agreement, thus validating the GIL approach. For further details on the validation study, refer to Bakuckas.[16] The commercially available finite element program ABAQUS 5.6 (Ref. 17) was used for the current analysis. In the first step (global level) of the GIL approach, an analysis of the plate subjected to the prescribed loading conditions is conducted. For the cases analyzed here, due to symmetry in the geometry and loading, one quadrant of the plate was modeled. The global model typically contained 1200 20-noded brick elements. In the next stage (intermediate level), an analysis is conducted of the area of interest, in these cases the higher stress gradient region near the hole, using a more refined mesh. The intermediate model typically consisted of 5000 20-noded brick elements. The boundary conditions for the intermediate model were taken from the global model using the submodeling features in ABAQUS. In the final stage (local level), an analysis is conducted that is even more focused on the region of interest, in these cases the region around the crack front. A very refined mesh with elements orthogonal to the crack front was used. The boundary conditions for the local model were taken from the global model using the submodeling features in ABAQUS.

From local models, the J-integral was calculated along the crack front using the equivalent domain integral method (EDIM). For cases where there is no mixed mode fracture and assuming a plane strain elastic material response, the mode I SIF at any point along the crack front can be calculated from the J-integral by

$$K_I = \sqrt{JE/(1-\nu^2)} \tag{8}$$

It should be noted that, for small cracks at locations 1 and 2 (Fig. 1f), the full GIL approach (three levels) was required. For larger crack sizes at locations 3, 4, and 5, a two-level global-local hierarchical approach was sufficient to obtain acceptable results. In the two-level approach, the global model had approximately 4500 20-noded brick elements, and the local model had 5600 20-noded brick elements.

Results and Discussion

The parameters in Table 1 were varied to the specified values, yielding a total of 117 solutions. All results are reported by Rahman et al.[14] A representative selection is presented here to illustrate the essential features of cracks at countersunk rivet holes. The effect of the shape of the crack, the location the crack, the length of straight-shank hole, and the loading condition are illustrated. It was noted

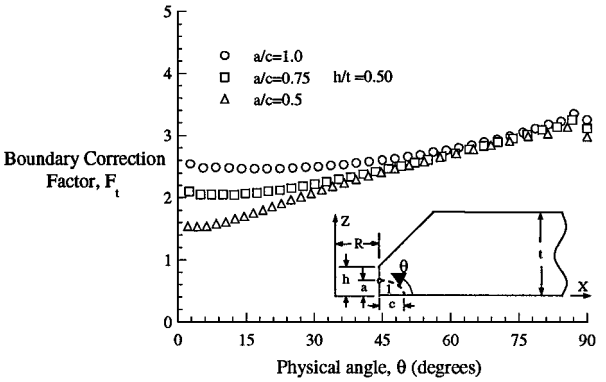

Fig. 3 Effect of crack shape on boundary correction factors.

that, although the value of the boundary correction factor was a function of the loading condition, the trends exhibited by the solution were similar for each loading condition. In the following discussion, the emphasis is placed on the tension loading condition results, but the arguments apply equally well to the bending and wedge loading cases.

Effect of Crack Shape on Boundary Correction Factor

The boundary correction factors (BCF) under tension, F_t, for cracks at location 1 with $h/t = 0.50$ are shown in Fig. 3 as a function of the physical angle, θ. The shape of the elliptical cracks was varied from $a/c = 1$, 0.75, and 0.5. The value of a was held constant and the value of c varied to obtain the desired a/c ratio. In general, for all three a/c ratios, the value of the boundary correction factor increased with an increase in the physical angle (i.e., as one moved along the crack front from the inner surface of the plate to the hole boundary). As shown in Fig. 3, for small values of θ, (near the inner or faying surface of the plate), the values of boundary correction factors increased directly with the value of a/c. Smaller a/c values mean a larger value c, and thus the crack front is further away from the corner and, therefore, has a relatively lower BCF. As the value of θ increased (at parts nearer the boundary of the hole), the solutions for the three values of a/c merged. This result is expected since all three cracks considered here have the same value of a and, consequently, approach the same point on the hole boundary. At $\theta = 90$ deg, i.e., at the hole boundary, the BCF is highest for each of the three crack shapes. Similar trends were observed at other crack locations and h/t ratios.

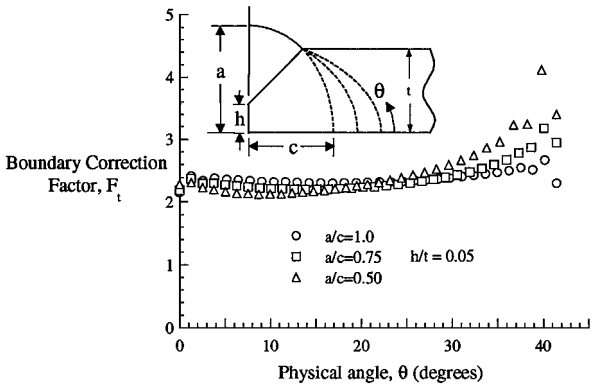

Fig. 4 Effect of crack shape in breakthrough cracks.

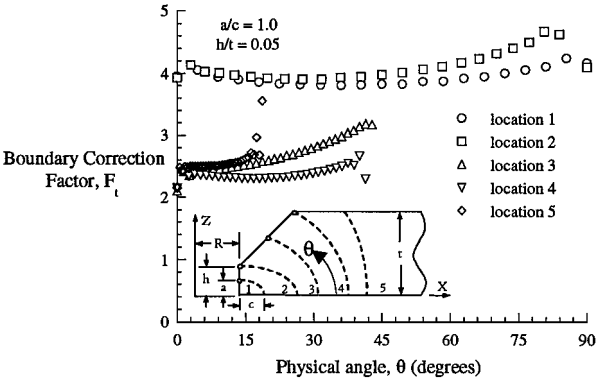

Fig. 5 Effect of crack location on boundary correction factors: h/t = 0.05.

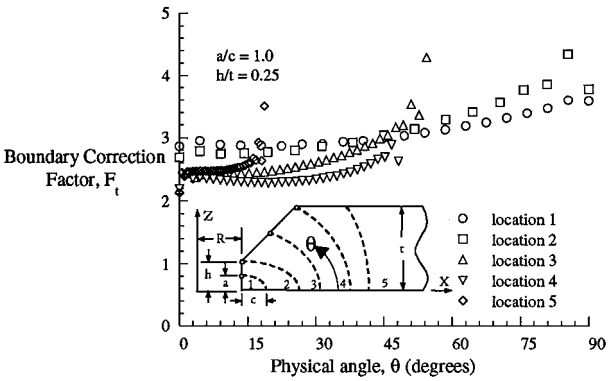

Fig. 6 Effect of crack location on boundary correction factors: h/t = 0.25.

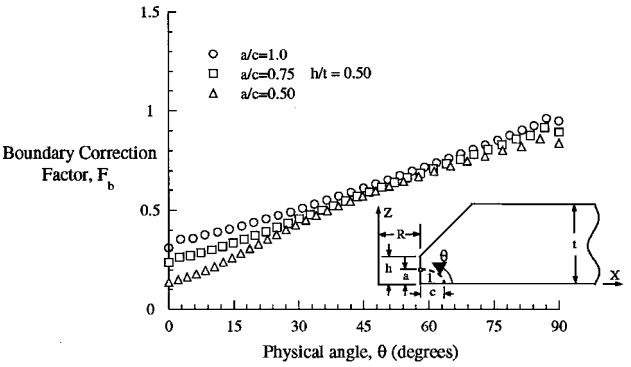

Fig. 7 Boundary correction factors for bending loading conditions.

The effect of a/c ratio on the breakthrough cracks (at locations 4 and 5) is slightly different than those discussed earlier. For breakthrough cracks the crack fronts do not intersect the straight shank hole boundary but terminate at a point on the outer surface. The boundary correction factor are highest at these points where the crack intersects. A typical example is shown in Fig. 4. Here for $h/t = 0.05$, boundary correction factors are plotted for three crack shapes with a/c of 1, 0.75, and 0.50. These cracks are at location 4. To obtain the different crack shapes, a and c were adjusted such that the required a/c was obtained and the crack front passed through the lip of the countersunk. As before, the crack fronts with larger a/c ratios are closer to the hole boundary. In this case, however, at $\theta = 0$ deg the crack front is relatively far from the hole, so the effect of the hole on the boundary correction factor is almost negligible. On the other hand, at higher values of θ, as one moves along the crack front towards the outer surface boundary, the BCF diverge from each other, and, actually, the crack front with the lowest a/c value results in the highest boundary correction factor. This can be explained by observing that for these cracks, the uncracked material in front of the crack front forms a sharp angle where the crack front meets the outer surface. This angle is sharper as a/c ratio gets smaller.

Effect of Crack Location on Boundary Correction Factor

The boundary correction factors for cracks at the five locations, as a function of the physical angle, θ for $a/c = 1$ and $h/t = 0.05$ under tension loading, are shown in Fig. 5. In general, at each location, as one moves along the crack front from the inner surface of the plate towards the outer surface and hole boundaries (increasing θ), the value of the boundary correction factor increases. Thus, for all crack locations, the hole and outer surface boundaries have more of an effect on the value of the boundary correction factor than the inner surface boundary of the plate. For crack locations 1 and 2, the entire crack front is near the hole (compared to the other three locations) and the values of the boundary correction factor are higher. The highest value for boundary correction factors were calculated for cracks at location 2 at points on the crack front at larger values of θ, where the crack front meets the countersunk hole at the knee. Here the crack front intersects the hole boundary at a point of abrupt geometry change, consequently the value of the BCF is higher. In general, the farther a point on the crack front is away from the boundary, the lower is the value of the boundary correction factor. Similar trends were observed at different a/c and h/t ratios. The boundary correction factors under tension, F_t, as a function of the physical angle, θ, for $a/c = 1$ and $h/t = 0.25$ are shown in Fig. 6. Similar trends are observed as for the case with $h/t = 0.25$ shown in Fig. 5. That is, the boundary correction factor increase with an increase in the physical angle, and the values are highest for the crack fronts nearer the hole at locations 1 and 2. In comparing the results from Figs. 5 and 6, the effect of changing h/t on the boundary correction factor is evident. For crack locations, 3, 4, and 5, where the influence of the hole is less, the values of F_t are similar for the two values of h/t. However, at crack locations 1 and 2, the change in h/t results in a significant overall increase in the boundary correction factors. For $h/t = 0.05$, Fig. 5, a near knife edge condition exists resulting in a much higher stress gradient region in the straight shank portion of the hole compared to the case of $h/t = 0.25$. Also in this case where $h/t = 0.05$, the a and c are very small and hence the entire crack is very close to the hole boundary. Consequently, the boundary correction factors for the crack fronts near the hole boundary at locations 1 and 2 are higher for $h/t = 0.05$ than for $h/t = 0.25$.

Effect of Applied Loading on Boundary Correction Factors

The boundary correction factors under bending F_b and wedge loading F_w as a function of the physical angle θ for h/t of 0.05 are shown in Figs. 7 and 8, respectively. Each figure shows the results for values of $a/c = 1$, 0.75, and 0.5. Whereas the magnitude of the BCF depends on the loading mode, the trend observed for both the bending and wedge loading is similar to that for the tension load case shown in Fig. 3. The values of boundary correction factors increase with increases in the physical angle, moving along the crack front from the inner surface toward to hole boundary. Additionally, for small values of θ, near the inner surface, the boundary correction factor increases as the value of a/c increases. At larger

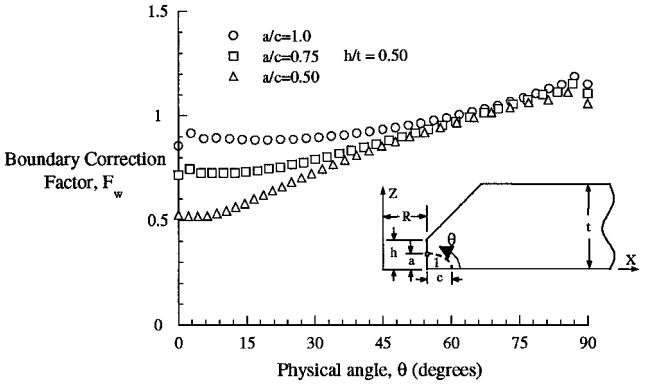

Fig. 8 Boundary correction factors for wedge loading conditions.

values of θ, at points on the crack front near the hole boundary, the values of the solutions for each of the three a/c ratios merge.

Conclusions

The database of known stress-intensity factor (SIF) solutions of cracks emanating from countersunk rivet holes under tension, bending, and wedge load conditions has been expanded in this study. Results were generated for 117 different configurations. The crack size, shape, and location were selected to represent typical experimental observations. The crack shape was varied with the ratio of the elliptical crack length in the thickness direction to that in the width direction as $a/c = 0.5$, 0.75, and 1. The ratio of the length of the straight-shank portion of the hole to the plate thickness (h/t) was varied ranging from 0.05, 0.25, and 0.50. Cracks at five locations were analyzed: 1) corner crack passing through the middle of straight shank portion of the rivet hole, 2) corner crack passing through inner knee of the rivet hole, 3) breakthrough crack passing through the middle of the inclined surface of the rivet hole, 4) breakthrough crack passing through the upper knee of the rivet hole, and 5) through-the-thickness crack passing through the inner and outer surfaces of the plate.

A global-intermediate-local (GIL) hierarchical submodeling technique was used to generate the stress-intensity factor solutions. Representative results generated using the GIL approach are presented in this paper in terms of the boundary correction factors. The effect of the shape of the crack, the location of the crack, the height of the straight-shank portion of the countersunk rivet hole, and applied loading are presented. The boundary correction factor was determined along the crack front in terms of the physical angle measured from the inner surface of the plate to the given point on the crack front.

In general, the values of boundary correction factors increased as one moved along the crack front from the inner surface of the plate toward the hole boundary. For small physical angles, i.e., near the inner surface of the plate, the value of the boundary correction factor increased with an increase in the value of a/c. As the physical angle increased, i.e., at points on the crack front nearer the hole boundary, the boundary correction factor solutions for the three values of a/c merged. For the five crack locations considered, the inner surface of the plate had less of an influence on the boundary correction factor than the hole and outer surface boundaries. The values of the boundary correction factor were highest for the crack fronts closest to the hole boundary. The trends in the solutions were the same for the three loading conditions.

Acknowledgments

This research was supported in part by Grant 97-G-026 from the Federal Aviation Administration William J. Hughes Technical Center, Atlantic City International Airport, New Jersey. The computational effort was partially supported by Grant MSS960013P from the Pittsburgh Supercomputing Center.

References

[1]"A Report of the Airworthiness Assurance Working Group," Industry Committee on Widespread Fatigue Damage, Final Rept., Washington, DC, July 1993.

[2]Raju, I. S., and Newman, J. C., Jr., "Stress-Intensity Factors for a Wide Range of Semi-Elliptical Surface Cracks in Finite Thickness Plates," *Engineering Fracture Mechanics*, Vol. 11, No. 4, 1979, pp. 817–829.

[3]Packard, A. C., "Stress-Intensity Factors for Cracks with Circular and Elliptic Crack Fronts Determined by 3D Finite Element Methods," Rolls–Royce, TR PNR-90035, Darby, England, U.K., May 1980.

[4]Tan, P. W., Raju, I. S., Shivakumar, K. N., and Newman, J. C., Jr., "Evaluation of Finite Element Models and Stress-Intensity Factors for Surface Cracks Emanating from Stress Concentrations," *Surface-Crack Growth: Models, Experiments, and Structures*, ASTM STP 1060, American Society for Testing and Materials, Philadelphia, 1990, pp. 34–48.

[5]Gosz, M., and Moran, B., "Stress-Intensity Factors Along Three-Dimensional Elliptical Crack Fronts," Federal Aviation Administration, FAA Technical Rept. DOT/FAA/AR-96/97, Atlantic City, NJ, May 1998.

[6]Nishioka, T., and Alturi, S. N., "Analytical Solution for Embedded Elliptical Cracks and Finite Element-Alternating Method for Elliptical Surface Cracks Subjected to Arbitrary Loadings," *Engineering Fracture Mechanics*, Vol. 17, No. 3, 1983, pp. 247–268.

[7]Nishioka, T., and Alturi, S. N., "An Alternating Method for Analysis of Surface-Flawed Aircraft Structural Components," *AIAA Journal*, Vol. 21, No. 5, 1983, pp. 749–757.

[8]Tan, P. W., Bigelow, C. A., O'Donoghue, P. E., and Alturi, S. N., "Stress-Intensity Factor Solutions for Cracks at Countersunk Rivet Holes Under Uniaxial Tension," Federal Aviation Administration, FAA Technical Rept. DOT/FAA/CT-93/68, Washington, DC, Feb. 1994.

[9]Cruse, T. A., "Application of Boundary-Integral Equation Method to Three- Dimensional Stress Analysis," *Computer and Structures*, Vol. 3, No. 3, 1973, pp. 509–527.

[10]Heliot, J., Lebbens, R. C., and Pellissier-Tanon, A., "Semi-Elliptical Surface Cracks Subjected to Stress Gradients," *Fracture Mechanics, ASTM STP 677*, edited by C. W. Smith, American Society for Testing and Materials, Philadelphia, 1979, pp. 341–364.

[11]Zhao, W., Wu, X. R., and Tan, M. G., "Weight Function Method for Three-Dimensional Crack Problems," *Engineering Fracture Mechanics*, Vol. 34, No. 3, 1989, pp. 593–607.

[12]Zhao, W., Newman, J. C., Jr., Sutton, M. A., Wu, X. R., and Shivakumar, K. N., "Analysis of Corner Cracks at Hole by a 3-D Weight Function Method with Stresses from Finite Element Method," NASA TM-110144, July 1995.

[13]Piascik, R. S., and Willard, S. A., "The Characteristics of Fatigue Damage in the Fuselage Riveted Lap Splice Joint," NASA TP-97-206257, 1997.

[14]Rahman, A., Bakuckas, J., Bigelow, C., and Tan, P., "Boundary Correction Factors for Elliptic Surface Cracks Emanating from Countersunk Rivet Holes Under Tension, Bending, and Wedge Loading," Federal Aviation Administration, FAA Technical Rept. DOT/FAA/AR-98/37, Atlantic City, NJ, March 1999.

[15]Murakami, Y., *Stress Intensity Factor Handbook*, Vol. 2, Pergamon, Oxford, 1987.

[16]Bakuckas, J. G., Jr., "Comparison of Boundary Correction Factor Solutions for Two Symmetric Cracks in a Straight Shank Hole," Federal Aviation Administration, FAA Technical Rept. DOT/FAA/AR-98/36, Atlantic City, NJ, April 1999.

[17]"ABAQUS," Ver. 5.6, Hibbit, Karlsson, and Sorenson, Pawtaucket, RI, 1996.

S. Saigal
Associate Editor